Metastable States of Small-Molecule Solutions

Guangwen He,[†,‡] Reginald B. H. Tan,[‡,§] Paul J. A. Kenis,[†] and Charles F. Zukoski*[,†]

Department of Chemical & Biomolecular Engineering, University of Illinois at Urbana−Champaign, 600 South Mathews Avenue, Urbana, Illinois 61801, Department of Chemical & Biomolecular Engineering, National University of Singapore, 4 Engineering Drive 4, Singapore 117576, and Institute of Chemical & Engineering Sciences, 1 Pesek Road, Jurong Island, Singapore 627833

Received: July 8, 2007; In Final Form: August 20, 2007

Metastable states such as gels and glasses that are commonly seen in nanoparticle suspensions have found application in a wide range of products including toothpaste, hand cream, paints, and car tires. The equilibrium and metastable state behavior of nanoparticle suspensions are often described by simple fluid models where particles are treated as having hard cores and interacting with short-range attractions. Here we explore similar models to describe the presence of metastable states of small-molecule solutions. We have recently shown that the equilibrium solubilities of small hydrogen-bonding molecules and nanoparticles fall onto a corresponding-states solubility curve suggesting that with similar average strengths of attraction these molecules have similar solubilities. This observation implies that metastable states in small-molecule solutions may be found under conditions similar to those where metastable states are observed in nanoparticle and colloidal suspensions. Here we seek confirmation of this concept by exploring the existence of metastable states in solutions of small molecules.

I. Introduction

Metastable states occur when systems are trapped in local free energy minima for sufficiently long periods of time that they can be observed.[1] Some practical uses of these states include glasses and gels. Often these states are achieved with colloidal particles and can be seen in such diverse products as toothpaste, hand cream, paints, and car tires. Two types of metastable states are of interest here. The first are the liquid states often reported for protein and nanoparticle suspensions where a liquid−liquid phase separation (LLPS) is achieved by quenching a suspension rapidly below its solubility point. The second type of metastable state is a gel composed of a space-filling network in which the particles exhibit extremely sluggish self-diffusion. Typically a glass is thought of as being a metastable state where particle motion is very sluggish but the trapping mechanism is dominated by volume exclusion with the prototypical example being that of hard-sphere glasses. Gels, on the other hand, occur in systems where the particles experience attractions of sufficient magnitude that localization is the result of bond formation. Both of these states are commonly observed in colloidal suspensions. Here we explore their existence in small-molecule solutions.

Over a decade ago a flurry of activity established that systems containing hard spheres with short-range interactions do not show thermodynamically stable liquid states.[2−11] Extensive calculations for a variety of short-range pair potentials demonstrate that only two thermodynamically stable states (fluid and crystalline) exist when the range of the attractive pair potential is a small fraction of the hard-core size.[3−8] Developed for hard-core Yukawa and square-well fluids, these models have been applied to a variety of experimental colloidal and nanoparticle systems where the assumption is made that the pair potential can be considered in the pseudo-one-component limit as a potential of mean force.[2,9,11]

Making a connection between the predicted and measured solubilities requires the states of the solutions to be compared at the same strength of attraction relative to the average thermal energy of the system, kT, where k is Boltzmann constant and T is the absolute temperature of the system. The second virial coefficient of the nanoparticle or solute, an integral measure of strength and range of attraction, is often taken as a surrogate for well depth.[9] While this approach fails for long-range attractions, calculations show that as the range of interaction becomes a small fraction of the particle diameter, the solubility at a given second virial coefficient is a very weak function of the range of attraction.[3−8] Thus for systems that have short-range attractions the magnitude of the second virial coefficient correlates solubilities well. Systems that experience short-range attractions are predicted to have a metastable liquid−liquid phase separation that occurs at strengths of attraction that are larger than those required to produce crystals or at a lower temperature than the crystallization temperature.[3,9−11] These metastable liquid−liquid phase transitions are observed and the resulting supersaturated phases are sometimes remarkably resistant to nucleation of the stable crystal phase. Detailed measurements of rates of nucleation indicate that the rate of nucleation passes through a maximum near the metastable state of liquid−liquid coexistence.[12,13]

In agreement with model predictions for particles interacting with short-range attractions, a great deal of experimental data have accumulated showing that the solubilities for many proteins and nanoparticles under a broad range of solution conditions lie in a narrow band when plotted as a function of the second virial coefficient.[14,15] Thus, in agreement with predictions for centrosymmetric interaction potentials, the second virial coef-

* To whom correspondence should be addressed. Phone: (217) 333-7448. E-mail: czukoski@uiuc.edu.
† University of Illinois at Urbana−Champaign.
‡ National University of Singapore.
§ Institute of Chemical & Engineering Sciences.

10.1021/jp075314o CCC: $37.00
Published on Web 12/06/2007

ficient is the corresponding-states variable for solubility. However, the corresponding-states model also predicts that the critical point of the metastable liquid−liquid phase transition would also occur at the same volume fraction and second virial coefficient. This is rarely observed and can be understood if the systems being investigated interact with noncentrosymmetric and valence-limited pair potentials.[16−21] Interestingly, these variations in the pair potential do not disrupt the corresponding-states collapse of solubility when plotted as a function of second virial coefficient suggesting the metastable liquid−liquid phase transition is more sensitive to details of the pair potential than is the solubility. As a result, deviations from this corresponding-states model for the critical point provide insights about the anisotropic and valence limitations of the pair potentials while deviations from the corresponding-states collapse of solubility data may prove to be useful in the range of the pair potential.

While the second virial coefficient is a surrogate for the strength of attraction for particles interacting with short-range attractions, a priori prediction of the second virial coefficient remains difficult as this parameter is sensitive to continuous phase composition and solution temperature.[15] As a result, experimental measures of the strength of attraction are required to link continuous phase composition to protein and nanoparticle solubility.

In the study of metastable states there is equal interest with the second type of metastable state, the gel. Gels are states where long-range diffusion of the solute is greatly suppressed resulting in materials with elasticity and long stress relaxation times. Gels are observed in many colloidal systems at sufficiently large strengths of attraction and volume fractions.[22] Mode coupling theory (MCT) and its extensions[23−26] that link equilibrium microstructure to structural arrest based on particle localization by cages of nearest neighbors and by bond formation are used widely to describe gel formation. Alternative approaches capture the link of the onset of sluggish behavior or the gel point to the approach of the solute self-diffusivity to a uniformly small value.[27,28] Experimentally, for a limited series of systems, the gel line has been characterized relative to the solubility and liquid−liquid phase transition boundaries.[14,29]

The models used to describe metastable liquid−liquid phase transitions and gel formation are essentially independent of particle size and application of these models relies on the assumption that the experimental systems are in the pseudo-one-component limit. Recently, this led us to expand the region of application of the corresponding-states model for solubility to small molecules.[30] In particular we showed that the solubilities of small molecules—glycine, L-histidine, L-phenylalanine, paracetamol, and ibuprofen—occur at the same volume fraction as observed for proteins and other nanoparticles when compared at the same value of an integral measure of the strength of attraction. In our studies, rather than the second virial coefficient B_2, we chose the pair contribution of the scaled long-time self-diffusivity D_2—a quantity that is easily measured for small molecules and nanoparticles by using pulsed-field gradient spin−echo nuclear magnetic resonance (PGSE NMR).[31] In the dilute limit, this term is a hydrodynamically weighted measure of the strength of interaction. In the low volume fraction, ϕ, limit, the self-diffusivity of a solute molecule can be written as[32−35] $D_s = D_0(1 + D_2\phi)$ such that by measuring the concentration dependence of D_s one can extract D_2 from the knowledge of molecular volume. For a wide range of solute molecules, temperatures, and solvent compositions, we found that solubility correlates well with D_2. After establishing that the equilibrium properties of these small organic molecules are very similar to those of nanoparticles and proteins when compared at the same D_2, we began to look for evidence of metastable states in small-molecule solutions.

Metastable liquid−liquid phase transitions in small-molecule solutions are not often reported but are known to exist. In the pharmaceutical industry, these metastable states are long-lived and are detrimental to crystallization operations.[36−40] Reports of molecular gels are much rarer but there are examples from the molecular glass literature where the glass transition can be tracked as the fraction of solvent is increased from zero.[41,42]

The use of D_2 as a scale for the strength of intermolecular interactions provides us with a tool to compare locations of liquid−liquid phase transitions and gel boundaries in molecular and colloidal systems. Here we develop more complete state diagrams of small molecules where D_2 is used as a surrogate for strength of attraction and search for metastable states of small-molecule solutions of the hydrogen-bonding molecules ibuprofen, glycine, citric acid, and trehalose. We motivate our correlations by starting with spherically symmetric interaction energies where studies of anisotropy suggest that the correlation between B_2 and solubility are weakly impacted by anisotropy.[15,43] In the case of ibuprofen in ethanol/water mixtures, rapid quenching results in metastable liquid−liquid phase transitions, while glycine in aqueous solutions crystallizes upon cooling, aqueous citric acid solutions first separate into liquid phases, followed by formation of crystals, and aqueous trehalose solutions display liquid−gel phase transition phenomenon. Below we describe our observations and link these observations to metastable states in colloidal systems.

II. Experimental Section

Materials. Ibuprofen (Fluka, >99.0%) was dissolved into mixtures of deionized water (18 MΩ·cm, E-pure, Barnstead) and ethanol (AAPER Alcohol, Absolute 200 Proof). Glycine (Fluka, >99.0%), citric acid monohydrate (Sigma, 99.5−101%, A.C.S. Reagent), and D-(+)-trehalose dihydrate (Fluka, >99.0%) were dissolved in deionized water. Hen egg white lysozyme (Sigma, 3× recrystallized) was dissolved in sodium acetate buffer (0.1 M, pH 4.5) made by dissolving the appropriate amount of sodium acetate (Fluka, A.C.S. Reagent, Anhydrous) in a mixture of deionized water and acetic acid (Fisher Scientific, A.C.S. Reagent) in the presence of sodium chloride (Fluka, A.C.S. Reagent). All chemicals are used without further purification. Detailed solution compositions and experimental conditions are summarized in Table 1.

Measurement of Liquid−Liquid Phase Boundary with a Turbidity Meter. The experiments were carried out in a batch system. Prepared solutions were introduced into a 25-mL jacketed crystallizer (UFO Lab Glass) equipped with magnetic stirrer to ensure uniform mixing. The stirring speed was set at 300 rpm for all experiments. The solutions were heated to a temperature where the solutions appeared to be clear, and were held for 15 min to ensure thermo-equilibrium. They were then cooled down at a constant rate of 0.20 deg/min with a water circulator (Julabo FP50). Solutions were monitored in situ by a fiber optic colorimeter (Brinkmann Instrument PC920), and the turbidity of the solutions was recorded with a LABVIEW software module. The cloud-point temperature of each solution, i.e., the onset of LLPS, was taken as the temperature at which the turbidity of the solutions increased sharply.

Measurement of Self-Diffusivity with Pulsed-Field Gradient Nuclear Magnetic Resonance. The long-time self-diffusivities of various molecules in different solvents were measured by using ^{1}H pulsed-field gradient spin−echo (PGSE) NMR (time

TABLE 1: Solvent Compositions and Temperatures Used for the Self-Diffusivity Measurement of the Five Different Solutes Used in This Study[a]

solute	solvent compositions (temperatures in °C)	D_2 at different temperatures	molecular diameter (nm)
glycine	H_2O (5, 25, 40, 70)	−5.39, −3.91, −3.24, −2.35	0.48
citric acid	H_2O (10, 15, 20, 30)	−2.80, −2.70, −2.73, −2.63	0.65
ibuprofen	40/60 wt % EtOH/H_2O (15, 20, 25)	−24.27, −22.40, −16.89	0.76
	50/50 wt % EtOH/H_2O (10, 15, 20, 25)	−5.66, −5.08, −4.64, −4.22	
	60/40 wt % EtOH/H_2O (10, 15, 20, 25)	−4.05, −3.67, −3.39, −3.01	
	70/30 wt % EtOH/H_2O (15, 20, 25, 30)	−2.76, −2.21, −2.13,−2.10	
trehalose	H_2O (10, 20, 30, 40)	−4.77, −4.20, −4.01, −3.86	0.80
hen egg white lysozyme	0.1M NaAc, pH 4.5, and 3 wt/vol % NaCl (20, 25, 30)	−8.68, −5.94, −5.05	3.02
	0.1M NaAc, pH 4.5, and 5 wt/vol % NaCl (25, 30, 35)	−14.95, −12.88, −11.54	

[a] Values of D_2 are obtained from PGSE NMR experiments. The sizes of the molecules are estimated as described in the text.

scale: 1500 ms) with a 600 MHz spectrometer (Varian Unity Inova 600). The sample solution was injected to a spherical bulb microcell (Wilmad Glass, 5 mm), and then inserted into a NMR tube (Wilmad Glass, 5 mm) filled with D_2O (Sigma, Standard 99.98 ± 0.01 atom % D). This setup offers several advantages: (i) strong magnetic signals from the protonated molecules in the solvent (due to the use of ^1H probe) can be greatly reduced and (ii) material consumption can be minimized. Prior to each set of experiments at different temperatures, the NMR probe was calibrated by using reported self-diffusion coefficients of water at respective temperatures.[44−46]

III. Results and Discussion

Solution Phase Behavior. All molecules studied here are small organic molecules except for lysozyme, and they share many common characteristics such as the capacity to form hydrogen bonds. Solutions of each of these molecules, however, show drastically different phase behavior. In what is probably the most common method by which small hydrogen-bonding molecules phase separate, crystals are formed when aqueous glycine solutions saturated at 40 °C are quenched to a variety of temperatures ranging from 0 to 15 °C. We have been unable to observe LLPS in glycine solutions. In contrast, in a detailed study using process analytical techniques (PAT), Groen and Roberts reported that upon quenching a concentrated solution of citric acid, LLPS, is first observed but crystals form subsequently.[47] A third type of behavior is reported here for ibuprofen. Ibuprofen solutions made up in pure ethanol and ethanol/water mixtures separate into two liquid phases upon cooling. Crystallization from these liquid phases is exceedingly sluggish. Displaying a different type of metastable response, the protein hen egg white lysozyme (HEWL) exhibits relatively rapid crystallization, LLPS, and gelation depending on the specific continuous phase composition and temperature.[14] A further extreme of gelation can be found in aqueous trehalose solutions that gel if quenched to a temperature that is sufficiently low with a cryostat.[42,48] The temperatures to which the solutions must be quenched to produce the gel or glassy state may be so low that the solvent may also be immobile. We include this example to indicate what happens as we extrapolate our observations.

Molecular Self-Diffusion. For identical spherical particles that can be treated as diffusing in a continuous phase, the D_2 can be expressed as:[32−35]

$$D_2 = \int_2^\infty (-3 + A_{11} + 2B_{11}) g(r) r^2 \, dr + \int_2^\infty \left[\frac{A_{11} - A_{12} - B_{11} + B_{12}}{r} + \frac{1}{2}\left(\frac{dA_{11}}{dr} - \frac{dA_{12}}{dr} \right) \right] \times Q(r) g(r) r^2 \, dr \quad (1)$$

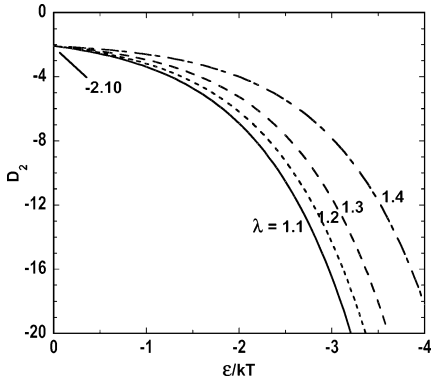

Figure 1. Plots of D_2 as a function of ϵ/kT for different λ.

where r is the normalized (by the radius of particle a) center-to-center spacing between the particles experiencing a pair potential $u(r)$, and the perturbation of the Maxwell−Boltzmann form of the pair distribution function $Q(r)$ and the mobility functions A_{11}, A_{12}, B_{11}, and B_{12} that are well-defined polynomials.[34,49] In the dilute limit, the pair correlation function $g(r)$ is written as:[50]

$$g(r) = \exp[-u(r)/kT] \quad (2)$$

if we approximate the pair interaction potential between the particles as a square-well form with

$$u(r) = \begin{cases} \infty & r < 2 \\ -\epsilon & 2 \le r < 2\lambda \\ 0 & r \ge 2\lambda \end{cases} \quad (3)$$

where ϵ and λ are the well depth and well width, i.e., the strength and range of interaction, respectively. Using the expressions of $Q(r)$, A_{11}, A_{12}, B_{11}, and B_{12} reported in the literature,[34,49] we find from eqs 1, 2, and 3 that

$$D_2 = \int_0^\infty \Omega \, dr + (e^{\epsilon/kT} - 1) \int_2^{2\lambda} \Omega \, dr = -2.10 + (e^{\epsilon/kT} - 1) \int_2^{2\lambda} \Omega \, dr \quad (4)$$

where

$$\Omega = \left[(-3 + A_{11} + 2B_{11}) + \left(\frac{A_{11} - B_{11} - A_{12} + B_{12}}{r} + \frac{1}{2}\frac{dA_{11}}{dr} - \frac{1}{2}\frac{dA_{12}}{dr} \right) Q(r) \right] r^2 \quad (5)$$

For hard spheres or in the high temperature limit ($\epsilon/kT = 0$), D_2 takes on a value of −2.10. In Figure 1 we have shown lines indicating the dependence of D_2 on temperature predicted by

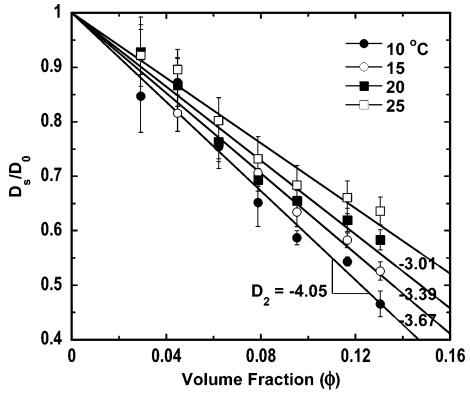

Figure 2. Scaled long-time self-diffusivities of ibuprofen in EtOH/H_2O (60/40 wt/wt %) as a function of solute volume fraction at 10, 15, 20, and 25 °C. The absolute concentration of ibuprofen is converted to particle volume fraction as described in the text. Values of D_2 are given by the slopes of the best linear fits.

eq 4 assuming that ϵ and λ are independent of temperature. The integral in the right-hand side of eq 4 give values of -0.1345, -0.2004, -0.2358, and -0.2564 for $\lambda = 1.1$, 1.2, 1.3, and 1.4, respectively.

The long-time self-diffusivities of ibuprofen in mixtures of ethanol and water were measured at different temperatures, and the values of D_2 were obtained from the slopes of the best linear fits of the scaled self-diffusivities plotted as a function of particle volume fraction (Figure 2). Similarly, the self-diffusivities and values of D_2 of glycine, citric acid, HEWL, and trehalose in different solvents at different temperatures were determined. When temperature decreases, the solute particles will spend a longer time to close together resulting in increasingly negative values of D_2 if they experience an attractive potential of mean force. We see such behavior in all the solutions under study (Figure 3). On the other hand, at the same experimental temperature, values of D_2 vary with the solvent composition (Figure 3b), implying that the composition of solvent is an important factor in determining the potential of mean force such that solvent composition can be used as a design tool for controlling phase transitions. The extent of attraction for these molecules is unknown. However, we expect the range of the attraction to be a small fraction of molecular diameter.[30] As a demonstration of how one can use D_2 measurements to estimate the strength of attraction, we first rearrange eq 4 to

$$\ln\left(\frac{D_2 + 2.10}{\int_2^{2\lambda} \Omega \, dr} + 1\right) = \frac{\epsilon}{kT} \tag{6}$$

where the values of ϵ/k could be obtained from independent measures of D_2 at different temperatures, if the range of attraction is given. Note that if the experimentally obtained D_2 values were less negative than the hard sphere value -2.10, eq 6 becomes physically meaningless. In such cases, we will take that those systems behave as hard spheres.

Attempts to determine ϵ/k from linear regression of several D_2 determined at different temperatures as shown in eq 6 result in very poor fits to the experimental data. This result suggests a significant temperature dependence of strength and/or range of interaction, i.e., if we choose to assume that the solutes interact with short-ranged, centrosymmetric square-well attractions, ϵ and λ are temperature dependent. For example, in the case of ibuprofen, if we extract values of ϵ/k from individual D_2 measurements at a certain temperature by assuming λ is constant (Table 2), we find a the strong dependence of ϵ on temperature and solvent composition, suggesting that experimental conditions and solvent composition can be used as design tools to tune particle interaction for the desired type of phase behavior. Nevertheless, the observed changes in D_2 cover a range of strengths of attraction where we anticipate the molecular solubility will change dramatically for the range of temperatures and solvent compositions investigated.

The values of D_2 for ibuprofen at the metastable liquid−liquid phase boundary are estimated by first measuring D_2 at several elevated temperatures, followed by extrapolating to the cloud-point temperatures. Due to lack of knowledge of temperature dependence of strength and range of interactions, the extrapolation is empirically done by linearly fitting the plots of D_2 as a function of inverse temperature. The values of D_2 of lysozyme solutions at the metastable liquid−liquid phase boundary and of aqueous trehalose solutions at the gel transition temperatures were obtained in a similar way. Experimental cloud-point temperatures of lysozyme solutions and gel transition temperatures of trehalose solutions were determined by Muschol and Rosenberger[51] and Cummins et al.,[42] respectively.

Generalized State Diagrams. By measuring the D_2 of the solutes in solutions of interest, we are able to construct a generalized phase diagram showing D_2 as a function of particle volume fraction ϕ where D_2 is taken as a measure of the strength of attraction in the place of dimensionless temperature (Figure 6). The detailed procedure to construct a generalized phase diagram based on D_2 was described in our previous study.[30] The molecules are treated as hard spheres interacting with each other in solution through a centrosymmetric square-well potential. The equilibrium solubility and nonequilibrium liquid−liquid phase boundaries are calculated by equating the osmotic pressures and chemical potentials of the respective phases of the solution.[30] We estimate the molecular volumes and particle sizes as described in our other work.[30] The particle size is calculated assuming the molecule is spherical in shape, yielding molecular diameters shown in Table 1.

As a guide to where gelation is expected to occur, we apply analytical mode coupling models that were recently developed for systems with attractions in the low volume fraction limit.[23−26] By assuming that density fluctuations are not important in determining the location of the gel line, Bergenholtz et al. derived a analytical solution for the location of the gel boundary for spherical particles interacting with square-well attraction of range λ based on mode coupling theory (MCT):[25]

$$\frac{12}{\pi^2}\phi(\lambda - 1)(e^{\epsilon/kT} - 1)^2 = 1.42 \tag{7}$$

By converting the well depth ϵ/kT to D_2 using eq 4, we are able to plot the MCT gel line in Figure 6b (for $\lambda = 1.1$).

The phase diagram depicted in Figure 6 captures essential features seen in a variety of theoretical and modeling studies.[3−9] These models assume the following: (i) the solute particles are spherical in shape, (ii) these particles have impenetrable hard cores, and (iii) they interact via the centrosymmetric square-well potential. The phase diagram shown in Figure 6 well describes the solubility boundary for a variety of molecules. Note that for $\lambda = 1.1$, the critical point is predicted to fall below the solubility curve, i.e., LLPS is expected to occur at D_2 values that are more negative than those characterizing the solubility. In addition, the gel boundary intersects the spinodal for LLPS at concentrations above the critical point for LLPS. A feature in common with many models for solubility is that over a relatively narrow range of change in D_2 (or ϵ/kT), the solubility changes dramatically.[9] While the solubility curve is insensitive

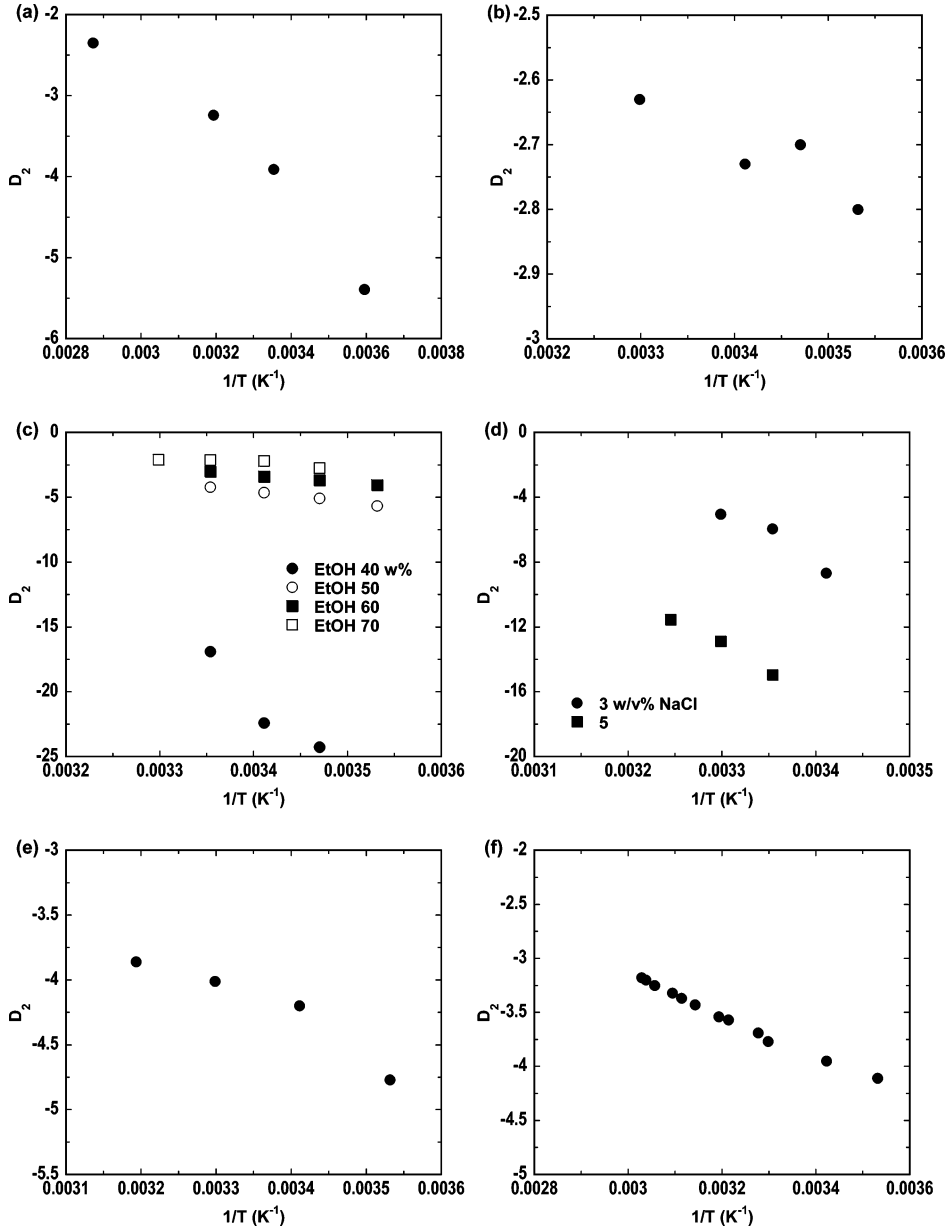

Figure 3. D_2 of various solute molecules in different solutions at different temperatures: (a) glycine in water; (b) citric acid in water; (c) ibuprofen in different solvent compositions of EtOH/H_2O; (d) hen egg white lysozyme in 0.1 M NaAc buffer (pH 4.5) in the presence of different concentrations of NaCl; (e) trehalose in water; and (f) an API in EtOH/H_2O (54.2/45.8 wt %). Note that (a)−(e) present experimental data obtained in this work and (f) presents data extracted from literature as described in the text.[38]

TABLE 2: Values of ϵ/k Extracted from Eq 6 for Ibuprofen in Different Solvents

solute	solvent composition	temp (°C)	ϵ/k (K)
ibuprofen	40/60 wt % EtOH/H_2O	15	1472.7
		20	1472.6
		25	1404.1
	50/50 wt % EtOH/H_2O	10	937.9
		15	905.6
		20	876.4
		25	840.9
	60/40 wt % EtOH/H_2O	10	776.5
		15	731.3
		20	692.0
		25	609.8

to λ, our calculations (not shown here) indicate that the value for D_2 at the critical point does vary with λ ranging from -4.17 for $\lambda = 1.1$ to -3.30 at $\lambda = 1.4$.

Recent theoretical and modeling studies suggest that for short-range attractions, anisotropy in the pair interaction potentials can alter the volume fraction and the strength of attraction at the critical point.[16−21] Sear[16] and Kern and Frenkel[17] pointed out that strongly directional interactions induced by "patchy" sites on the particle surface could alter the universality of the critical temperature, and further indicated that the critical temperature would be lower as the patches become smaller. Zaccarelli and co-wrokers[18−20] studied the phase diagrams of patchy particles using numerical simulation, and found that the liquid−liquid coexistence region shrinks as the maximum number of bonded particle interactions decreases. Despite changes in the location of the critical point, the solubility boundary is only weakly dependent on anisotropy.[15] On the other hand, Katsonis et al.[21] illustrated that non-monotonic potentials with varying strength of interaction can result in deviation from the law of corresponding-states solubility behavior.

Our purpose here is not to characterize the anisotropy or lack of valence in the interaction energies of the molecules studied. Instead our goal is to demonstrate that small molecules display

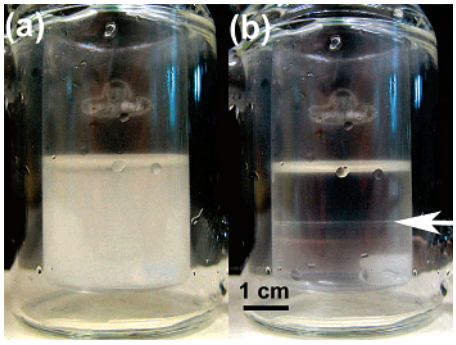

Figure 4. Solution of ibuprofen (200 g/kg solvent) in a mixture of EtOH and H_2O (50/50 wt/wt %) at 20 °C: (a) opaque solution, when the stirrer is on, and (b) two distinct homogeneous liquid layers, when the stirrer is off. The arrow indicates the liquid−liquid interface.

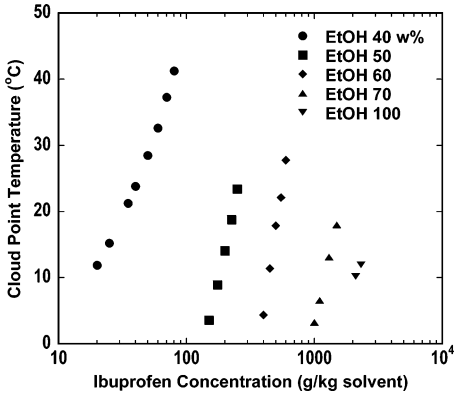

Figure 5. Cloud-point temperatures of solutions of ibuprofen in different mixtures of ethanol and water.

metastable sates that are similar to those seen in the colloidal and nanoparticle domain and that these metastable states occur at similar strengths of attractions as seen in the nanoparticle cases. However, these studies will be important as we consider the range of behaviors observed in our experimental systems.

Discussion on the Presence and Absence of Metastable States. Aqueous solutions of the amino acid glycine produce crystals upon cooling, without going through any other types of phase transitions. To be more accurate, in a very broad literature on the crystallization of glycine and in our hands, no other types of phase transitions are observed when glycine solutions are either concentrated or quenched in temperature to D_2 values well below where we would expect the LLPS following the predictions of square-well fluid models. At the same time the solubility of glycine is well described by the corresponding-states model. This result suggests that nucleation is rapid and metastable states cannot be seen. From this we conclude that slow nucleation of the crystalline phase must be a prerequisite to long-lived metastable states such as LLPS that we would be able to characterize and analyze.

On quenching a concentrated aqueous citric acid solution undergoes a metastable LLPS. The liquid states are short-lived and are quickly overwhelmed by crystal nucleation.[47] Such two-liquid formation has been evidenced in the literature as a result of molecular cluster formation in the supersaturated solutions.[52] Citric acid displays a very high solubility in water, showing D_2 values that are reaching the hard sphere limit as the strength of attraction ϵ approaches zero such that D_2 has weak temperature variation (Figure 3b).

The solutions of ibuprofen/ethanol/water present clear evidence of changes in interaction potential as the ethanol−water ratio is altered. We observe liquid−liquid phase transitions on cooling in pure ethanol and in ethanol−water mixtures. In pure water, crystals form upon quenching. In pure ethanol solutions as the temperature is quenched, a liquid−liquid phase transition occurs. In ethanol/water mixtures, the critical point of the metastable liquid−liquid phase boundary moves to lower concentrations as the water content is increased. To verify what type of phase transition induced the cloudiness of the solution, we stopped the active stirring of the solution. The opaque solution gradually separated into two distinct homogeneous liquid layers (Figure 4), implying that the cloudiness was caused by the onset of LLPS but not by crystal nucleation.

The cloud-point temperatures of ibuprofen solutions were taken as the temperatures at which the solutions suddenly turned opaque. At a given temperature, the amount of ibuprofen needed to cloud the solution differs by orders of magnitude as the ethanol content is varied (Figure 5). We dropped ibuprofen crystals into the two liquid phases that were separated carefully using a pipet and found the crystals dissolved in the upper layer while they grew in the lower layer, which confirmed the metastability of this liquid phase with respect to crystallization. The phase separation here is complicated by the ability of the water and ethanol to partition at the point of phase separation. Our studies show that the less dense phase is rich in ethanol and ibuprofen. Up to the point of phase separation, however, the solutions are macroscopically homogeneous. As a result, up to the phase transition, we treat the ibuprofen as a pseudo-one-component system.

Of particular interest is that although the location of the critical point for the phase separation for the ibuprofen appears to shift toward lower volume fraction with increasing water content, when compared in a D_2 generalized phase diagram, all solubilities fall on the corresponding-states curve observed for small molecules and proteins. The simulations of Katsonis et al.[21] suggest that if this correlation is observed, the particles interact with a centrosymmetric pair potential indicating that the observed changes in the location of the LLPS with water concentration are unlikely to be associated with noncentrosymmetric pair potentials but instead may reflect changes in the effective valency of the ibuprofen crystals as the water content is increased.

Ibuprofen is an aromatic compound with a *phenyl* ring, para-substituted with a propionic acid group and an isobutyl group. The molecular structure makes ibuprofen far from being a good idealization of a hard-core spherical particle interacting with a centrosymmetric pair potential. Moreover, the interactions between ibuprofen particles are predominated by hydrogen bonding, which is highly directional and also inevitably influenced by the solvent molecules ethanol and water, both capable of forming hydrogen bonds as well. The experimental data presented in Figure 5 show that the critical point of the liquid−liquid coexistence curve shifts toward lower ibuprofen concentrations as the water content in the solvent increases. We hypothesize the following explanation for this observation: a water molecule can form four hydrogen bonds with its neighbors, while hydrogen bonding between ethanol molecules is not as effective as in water due to the fact that only the hydrogen atom of the OH group in each ethanol molecule carries sufficient positive charge. Only two hydrogen bonds are formed between ethanol molecules where the oxygen atom is acting as both a proton donor and a proton acceptor.[53] Furthermore, the hydrogen bonds formed by water molecules are stronger than those formed by ethanol molecules. Thus water molecules are more likely to interact with ibuprofen molecules through hydrogen bonding. As the water content in the solvent increases, the solute−solvent

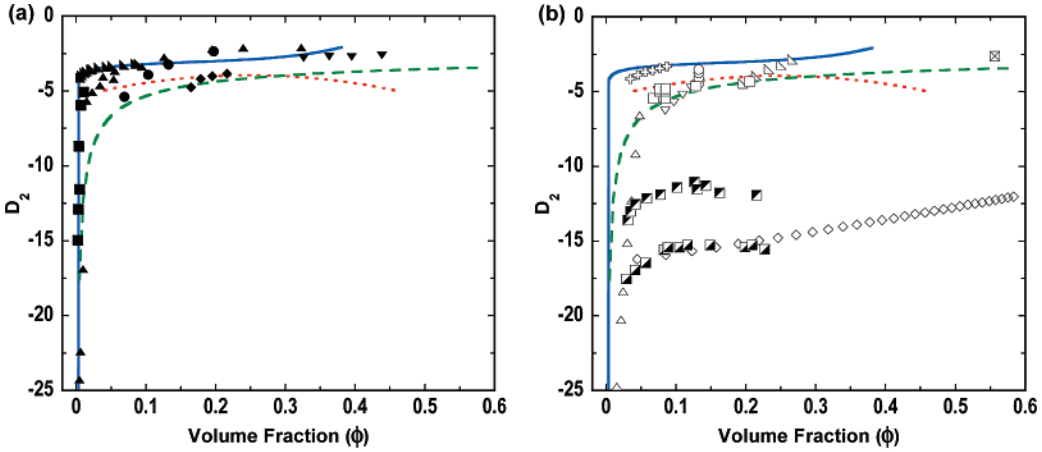

Figure 6. Generalized phase diagram for a variety of molecules in D_2 space. Various symbols are experimental (a) solubility data, and (b) data corresponding to metastable states. (a) The closed upper triangles, circles, diamonds, lower triangles, and squares are solubility data of ibuprofen, glycine, trehalose, citric acid, and lysozyme from literature.[47,54,59−61] (b) The open circles stand for conditions where glycine crystals form in aqueous solution. The open upper, lower, and right-angle triangles correspond to LLPS data of ibuprofen in ethanol/water mixtures with ethanol content of 40, 50, and 60 wt %, respectively. The open diamonds represent the glass transition point for aqueous trehalose solutions. The upper and lower half-filled squares correspond to LLPS data of lysozyme solutions in the presence of 3 and 5 wt/vol % NaCl, respectively.[51] The open squares are gelation data of lysozyme taken from literature[14] and expressed into D_2. The cross-square corresponds to LLPS data of aqueous citric acid solution.[47] The open crosses present LLPS data of an API extracted from literature as described in the text.[38] The solid, short-dashed, and long-dashed lines are the model solid−liquid, liquid−liquid, and MCT gel boundaries for ranges of interaction $\lambda = 1.1$. Experimental conditions are specified in Table 1.

interactions become stronger, reducing the available interaction sites between solute particles and resulting in a decrease in maximum number of bonded interactions between ibuprofen molecules. The result would be a shift of critical point to lower concentrations and lower temperatures or dimensionless temperatures.[18−20]

Similar stable LLPS have been observed in a variety of small-molecule solutions.[36−40] In a well-defined set of measurements where the solubility and spinodal of an active pharmaceutical ingredient (API) has been characterized, Veesler and co-workers[37−40] observed crystals nucleated at the dense liquid drops and the dilute phase boundary. This compound is not available to us. To make comparisons with the results reported by Veesler and co-workers,[37−40] we assume that this compound satisfies the corresponding-states solubility curve, and using an effective particle diameter of 1.06 nm calculated by assuming the crystal density as 1.6 g/cm^3, we extract the D_2 dependence on temperature from the dependence of solubility on temperature (solubility data of Form I are used), shown in Figure 3f. Knowing D_2 as a function of temperature we then are able to plot the experimentally measured location of LLPS as a function of volume fraction using the procedure as mentioned above (Figure 6b).

The values of D_2 of trehalose (Figure 3e) are very close to those of hard spheres echoing the tremendous solubility of trehalose in water.[54] In determining values of D_2 for aqueous trehalose solutions at the gel/glass line, we are only able to measure D_2 at elevated temperatures far from glass transition temperatures. Thus we are extrapolating a large temperature range that may not be physically reasonable but may provide a rough guide on the location of the gel/glass line of trehalose solutions (Figure 6b, open diamonds) on the generalized phase diagram. That trehalose solutions bypass all other solution states and gel upon deep quench may be an indicator of sluggish nucleation. As shown in Figure 6b, the extrapolation to D_2 at the gel (or glass) point yields D_2 values similar to those expected for short-range interactions.

There have been a variety of studies on Low Molecular Weight Organic Gelators (LMOGs) in the literature that induce formation of three-dimensional structural networks, i.e., organogels.[55−58] The wide diversity of the structures of LMOGs that directly concern how they pack in the assemblies plays an important role on the gelation properties. Two anthracene derivatives, one has two longish hydrocarbon tails attached white the other has short tails, were found to behave differently. The former always gels while the latter will gel or crystallize.[56−58] The long tails that may be detrimental to assembly efficiency and efficacy are thought to slow down crystal nucleation and thus assist gelation. The LMOG literature is replete with molecules that form gels at mass concentrations of a few percent. These materials tend to form ribbons and other extended, pseudo-one-dimensional structures which fill space and result in gelation. We anticipate that these materials will show very negative D_2 values indicative of strong attractions. The studies on the two anthracene molecules indicate that suppressing the ability of the system to crystallize is important to seeing gelation at such low solute volume fractions.

The generalized phase diagram depicted in Figure 6 demonstrates that the solubilities of all the molecules of interest fall into a narrow range of D_2, implying that the equilibrium phase behavior is rather similar for a variety of molecules when compared on the same basis. One can also see that the metastable states such as LLPS and gels in small-molecule solutions occur at strengths of attraction in a similar range as those seen in nanoparticle suspensions. However, the metastable phase transitions occur in a more unpredictable way suggesting that details in interaction potential such as limited valence and anisotropic interactions play an important role in nonequilibrium phase behavior.

Rate of Nucleation. A variety of phase behavior can be observed in small-molecule solutions: (i) Solutes like glycine that crystallize easily without displaying LLPS (in these systems the complete absence of a metastable LLPS may arise due to an enhanced crystal nucleation rate at conditions close to the critical state);[12] (ii) solutes like citric acid and Veesler's API that go through LLPS followed by the onset of nucleation; and (iii) solutes like ibuprofen that undergo LLPS (here crystal nucleation is sufficiently slow that the metastable liquids can

easily be observed). Often, the resulting phases are long-lived and resistant to crystallization. Solutes in type (ii) fit themselves nicely between types (i) and (iii), pointing to the significance of kinetic effects—either rapid formation of the liquid phases or slow crystal nucleation. These kinetic phenomena have seen limited study. (iv) In the extreme case of sluggish nucleation and limited number of bonds, gels are observed for solutes such as trehalose. Similarly, LMOGs are designed in a way that they cannot crystallize nor phase separate, suggesting that they form a very limited number of bonds and thus form gels.[55]

The differences in rates of nucleation for solutions containing solutes that fall into class (ii) may be interpreted through the theory of sequential yet superimposed density and structure fluctuations proposed by Vekilov.[12] The density fluctuation may result in dense liquid phase whose lifetime and relative metastability depend on the system itself. The dense liquid phase in citric acid solutions, which is metastable to both the low-density phase and crystals, displays a short-lived behavior.[12] In ibuprofen solutions, the metastability of the liquid phases with respect to crystals is extremely long-lived. The phase-separated liquid phases have remained homogeneous now for about 1 year at room temperature. The arrest of crystal nucleation in ibuprofen solutions could also be due to the change of the solution medium such as viscosity.[12,40] Gel and glass transitions in aqueous trehalose solutions with different water contents are observed without undergoing any other phase transitions.[42,48]

Note that in the above case studies of ibuprofen and trehalose solutions, the rate of nucleation is not accelerated even when gel formation or LLPS are observed, i.e., we are working with systems that nucleate in a sluggish manner. For these systems, it is straightforward to quench to conditions where solute molecules display strong attractions while avoiding nucleation.

IV. Conclusion

In this work we explored the existence of metastable phase transitions such as liquid−liquid phase separation and gel formation in small-molecule solutions. Our results are aided by our ability to compare states of solutions at similar values of the strength of intermolecular attraction as characterized by D_2. As a result we can develop generalized phase diagrams, which allow comparison of both small-molecule and nanoparticle solutions. Our studies show that while the equilibrium behavior of the solutes is similar, i.e., they have similar solubilities at similar D_2 values, the metastable states seen on quenching below the solubility boundary are variable. Several explanations drawn largely from studies motivated by colloidal and nanoparticle systems are seen to potentially capture the observed trends. These include anisotropic and valence-limited interactions. However, much more work is required to understand how these models can be linked to the observed states. Our studies also point to the limited understanding we have of the nucleation of equilibrium states in nanoparticle and small-molecule solutions.

Acknowledgment. This work is financially supported by the Agency for Science, Technology and Research (A*STAR), Singapore. The authors would like to thank Dr. Paul Molitor (UIUC) for his assistance in the NMR experiments.

References and Notes

(1) Debenedetti, P. G. *Metastable Liquids*: *Concepts and Principles*; Princeton University Press: Princeton, NJ, 1995.
(2) Gast, A. P.; Hall, C. K.; Russel, W. B. *J. Colloid Interface Sci.* **1983**, *96*, 251−267.
(3) Hagen, M. H. J.; Frenkel, D. *J. Chem. Phys.* **1994**, *101*, 4093−4097.
(4) Vega, L.; De Miguel, E.; Rull, L. F.; Jackson, G.; McLure, I. A. *J. Chem. Phys.* **1991**, *96*, 2296−2305.
(5) Heyes, D. M.; Aston, P. J. *J. Chem. Phys.* **1992**, *97*, 5738−5748.
(6) Lomba, E.; Almarza, N. G. *J. Chem. Phys.* **1994**, *100*, 8367−8372.
(7) Pagan, D. L.; Gunton, J. D. *J. Chem. Phys.* **2005**, *122*, 184515.1−184515.6.
(8) Liu, H.; Garde, S.; Kumar, S. *J. Chem. Phys.* **2005**, *123*, 174505.1−174505.4.
(9) Rosenbaum, D.; Zamora, P. C.; Zukoski, C. F. *Phys. Rev. Lett.* **1996**, *76*, 150−153.
(10) Lomakin, A.; Asherie, N.; Benedek, G. B. *J. Chem. Phys.* **1996**, *104*, 1646−1656.
(11) Haas, C.; Drenth, J. *J. Phys. Chem. B* **1998**, *102*, 4226−4232.
(12) Vekilov, P. G. *Cryst. Growth Des.* **2004**, *4*, 671−685.
(13) Pan, W.; Kolomeisky, A. B.; Vekilov, P. G. *J. Chem. Phys.* **2005**, *122*, 174905.1−174905.7.
(14) Kulkarni, A. M.; Dixit, N. M.; Zukoski, C. F. *Faraday Discuss.* **2002**, *123*, 37−50.
(15) Rosenbaum, D.; Kulkarni, A. M.; Ramakrishnan, S.; Zukoski, C. F. *J. Chem. Phys.* **1999**, *111*, 9882−9890.
(16) Sear, R. P. *J. Chem. Phys.* **1999**, *111*, 4800−4806.
(17) Kern, N.; Frenkel, D. *J. Chem. Phys.* **2003**, *118*, 9882−9889.
(18) Zaccarelli, E.; Buldyrev, S. V.; Nave, E. L.; Moreno, A. J.; Saika-Voivod, I.; Sciortino, F.; Tartaglia, P. *Phys. Rev. Lett.* **2005**, *94*, 218301.1−218301.4.
(19) Zaccarelli, E.; Saika-Voivod, I.; Moreno, A. J.; Nave, E. L.; Buldyrev, S. V.; Sciortino, F.; Tartaglia, P. *J. Phys.*: *Condens. Matter* **2006**, *18*, S2373−S2382.
(20) Bianchi, E.; Largo, J.; Tartaglia, P.; Zaccarelli, E.; Sciortino, F. *Phys. Rev. Lett.* **2006**, *97*, 168301.1−168301.4.
(21) Katsonis, P.; Brandon, S.; Vekilov, P. G. *J. Phys. Chem. B* **2006**, *110*, 17638−17644.
(22) Russel, W. B.; Saville, D. A.; Schowalter, W. R. *Colloidal Dispersions*; Cambridge University Press: New York, 1989.
(23) Bengtzelius, U.; Götze, W.; Sjölander, A. *J. Phys. C*: *Solid State Phys.* **1984**, *17*, 5915−5934.
(24) Götze, W.; Sjölander, A. *Rep. Prog. Phys.* **1992**, *55*, 241−376.
(25) Bergenholtz, J.; Fuchs, M.; Voigtmann, T. *J. Phys.*: *Condens. Matter* **2000**, *12*, 6575−6583.
(26) Schweizer, K. S.; Saltzman, E. J. *J. Chem. Phys.* **2003**, *119*, 1181−1196.
(27) Foffi, G.; De Michele, C.; Sciortino, F.; Tartaglia, P. *Phys. Rev. Lett.* **2005**, *94*, 078301.1−078301.4.
(28) Kaufman, L. J.; Weitz, D. A. *J. Chem. Phys.* **2006**, *125*, 074716.1−074716.11.
(29) Jansen, J. W.; de Kruif, C. G.; Vrij, A. *J. Colloid Interface Sci.* **1986**, *114*, 481−491.
(30) He, G.; Tan, R. B. H.; Kenis, P. J. A.; Zukoski, C. F. *J. Phys. Chem. B* **2007**, *111*, 12494−12499.
(31) Price, W. S. *Concepts Magn. Reson.* **1997**, *9*, 299−336.
(32) Batchelor, G. K. *J. Fluid Mech.* **1976**, *74*, 1−29.
(33) Batchelor, G. K. *J. Fluid Mech.* **1983**, *131*, 155−175.
(34) Cichocki, B.; Felderhof, B. U. *J. Chem. Phys.* **1988**, *89*, 3705−3709.
(35) Cichocki, B.; Felderhof, B. U. *J. Chem. Phys.* **1990**, *93*, 4427−4432.
(36) Bonnett, P. E.; Carpenter, K. J.; Dawson, S.; Davey, R. J. *Chem. Commun.* **2003**, *6*, 698−699.
(37) Veesler, S.; Lafferrère, L.; Garcia, E.; Hoff, C. *Org. Process Res. Dev.* **2003**, *7*, 983−989.
(38) Lafferrère, L.; Hoff, C.; Veesler, S. *J. Cryst. Growth* **2004**, *269*, 550−557.
(39) Deneau, E.; Steele, G. *Org. Process Res. Dev.* **2005**, *9*, 943−950.
(40) Veesler, S.; Revalor, E.; Bottini, O.; Hoff, C. *Org. Process Res. Dev.* **2006**, *10*, 841−845.
(41) Magazù, S.; Maisano, G.; Migliardo, P.; Tettamanti, E.; Villari, V. *Mol. Phys.* **1999**, *96*, 381−397.
(42) Cummins, H. Z.; Zhang, H.; Oh, J.; Seo, J.-A.; Kim, H. K.; Hwang, Y.-H.; Yang, Y. S.; Yu, Y. S.; Inn, Y. *J. Non-Cryst. Solids* **2006**, *352*, 4464−4474.
(43) Dixit, N. M.; Zukoski, C. F. *J. Chem. Phys.* **2002**, *117*, 8540−8550.
(44) Millis, R. *J. Phys. Chem.* **1973**, *77*, 685−688.
(45) Easteal, A. J.; Price, W. E.; Woolf, L. A. *J. Chem. Soc., Faraday Trans. 1* **1989**, *85*, 1091−1097.
(46) Holz, M.; Heil, S. R.; Sacco, A. *Phys. Chem. Chem. Phys.* **2000**, *2*, 4740−4742.
(47) Groen, H.; Roberts, K. J. *J. Phys. Chem. B* **2001**, *105*, 10723−10730.
(48) Chen, T.; Fowler, A.; Toner, M. *Cryobiology* **2000**, *40*, 277−282.
(49) Jeffrey, D. J.; Onishi, J. *J. Fluid Mech.* **1984**, *139*, 261−290.

(50) Hansen, J. P.; McDonald, I. R. *Theory of Simple Liquids*, 3rd ed.; Academic Press: London, UK, 2006.

(51) Muschol, M.; Rosenberger, F. *J. Chem. Phys.* **1997**, *107*, 1953−1962.

(52) Mullin, J. W.; Leci, C. L. *Philos. Mag.* **1969**, *19*, 1075−1077.

(53) Franks, F.; Ives, D. J. G. *Q. Rev. Chem. Soc.* **1966**, *20*, 1−44.

(54) Lammert, A. M.; Schmidt, S. J.; Day, G. A. *Food Chem.* **1998**, *61*, 139−144.

(55) Abdallah, D. J.; Weiss, R. G. *Adv. Mater.* **2000**, *12*, 1237−1247.

(56) Placin, F.; Desvergne, J.-P.; Lassègues, J.-C. *Chem. Mater.* **2001**, *13*, 117−121.

(57) Kato, T.; Kutsuna, T.; Yabuuchi, K.; Mizoshita, N. *Langmuir* **2002**, *18*, 7086−7088.

(58) Pozzo, J.-L.; Desvergne, J.-P.; Clavier, G. M.; Bouas-Laurent, H.; Jones, P. G.; Perlstein, J. *J. Chem. Soc., Perkin Trans. 2* **2001**, 824−826.

(59) Khalifeh, I. Thermodynamic Evaluation of Ibuprofen Solubility in Aqueous and Non-Aqueous Cosolvent Systems. Ph.D. Thesis, Purdue University, 2000.

(60) Fasman, G. D., Ed. *Handbook of Biochemistry and Molecular Biology*; Physical and Chemical Data, Vol. I; CRC Press: Cleveland, OH, 1975.

(61) Forsythe, E. L.; Judge, R. A.; Pusey, M. L. *J. Chem. Eng. Data* **1999**, *44*, 637−640.